Available online at www.sciencedirect.com

ScienceDirect

journal homepage: www.elsevier.com/locate/he

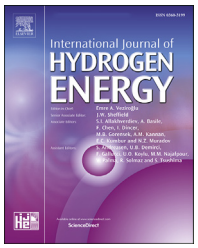

CO preferential oxidation on cordierite monoliths coated with CuO-CeO_2/SBA-15 catalysts. Further insights into the physico-chemical aspects of the catalytic behavior

*Albano M. Lacoste, Inés S. Tiscornia, Alicia V. Boix**

Instituto de Investigaciones en Catálisis y Petroquímica, INCAPE (FIQ, UNL-CONICET), 3000 Santa Fe, Argentina

ARTICLE INFO

Article history:
Received 1 March 2018
Received in revised form
11 May 2018
Accepted 21 May 2018
Available online 19 June 2018

Keywords:
Monolithic catalysts
CuO-CeO_2/SBA-15
COPrOx
Molar ratio CuO/CeO_2

ABSTRACT

CuO-CeO_2/SBA-15 catalysts deposited over cordierite monoliths were prepared to be tested in CO preferential oxidation (COPrOx). The influence of molar ratio between the CuO and CeO_2 active phases, their concentration, and the incorporation method into the mesoporous structure were analyzed. Powder catalysts were also studied in order to select the best formulations to coat the monolith walls. Four CuO/CeO_2 molar ratios over SBA-15 were obtained by incipient wetness impregnation technique (successive impregnation and co-impregnation). The CuO/CeO_2 = 0.55 ratio powder catalyst showed the best CO conversion in the temperature range studied, reaching 100% at 160 °C. The incorporation of active phases into the structured support produced similar or better catalytic behaviors. The addition of 10% CO_2 slightly decreased the CO conversion, while the addition of 10% H_2O partially deactivated the catalyst. The structured and powder catalysts prepared were characterized by N_2 sorption, TEM, SEM, XRD, XPS and TPR in order to identify and relate their physico-chemical properties with the catalytic behavior.

Introduction

The CO preferential oxidation reaction (COPrOx) is an important alternative to decrease CO content in the hydrogen-rich stream feed for PEM fuel cells that come from alcohol and hydrocarbon reforming. A CO concentration below 10 ppm is an acceptable value to prevent the cell anode from poisoning.

Several authors have developed successful catalysts based on precious or noble metals, achieving good results [1], but the high cost of these materials has led researchers to investigate other alternatives based on low-cost materials. Among the several catalysts that have been tested, materials based on copper-cerium oxides have demonstrated numerous interesting characteristics and have been widely studied. Their interactions, either geometric or electronic, have a key role in the catalytic performance for COPrOx [2]. For instance, Guo et al. [3] investigated the effect of the surface coverage of Cu atoms on the dispersion of CuO on CeO_2(rod) and the interfacial Cu-Ce interaction in CuCe(rod) catalysts. They reported an optimum range of copper content, where highly dispersed CuO strongly interacting with CeO_2(rod) greatly promoted the catalytic performance for COPrOx. Wang et al. [4] synthesized a series of CuO-CeO_2 samples using various methods and

* *Corresponding author*. INCAPE, Santiago del Estero 2829, 3000, Santa Fe, Argentina.
E-mail address: aboix@fiq.unl.edu.ar (A.V. Boix).
https://doi.org/10.1016/j.ijhydene.2018.05.122

different copper precursors, and they demonstrated that both variables had an important role in the catalytic behavior. In addition, Jampa and coworkers [5] analyzed mesoporous ceria catalysts with different percentages of Cu loading. They employed the deposition-precipitation method, obtaining a sample that achieved total CO conversion.

On the other hand, CuO-CeO_2 catalysts supported over different oxides (SiO_2, ZrO_2, Al_2O_3, etc.) were evaluated in CO oxidation and COPrOx reactions [6,7]. An interesting study of these oxides impregnated within SBA-15 was reported by Tang et al. [8]. The aim of their work was to investigate the solid state impregnation method to obtain CuO-CeO_2/SBA-15 catalysts. They explored the differences in the composition and structure between catalysts made by solid state impregnation and wet impregnation and correlated them with the COPrOx activity. Cecilia et al. [9] prepared porous clay heterostructures as support for CuO-CeO_2 based catalysts synthesized for the COPrOx reaction. They inserted pillars of silica or silica-zirconia in the interlayer space of the natural clay, which provided a high surface area that favored the active phases dispersion. Similarly, CuO/CeO_2 catalytic systems supported on Zr doped SBA-15 were synthesized and studied by Reyes-Carmona et al. [10].

It is known that the use of structured systems in numerous reactions enables their practical applications due to their low pressure drops, resistance to attrition and robustness. In the last decades, the development of monolithic catalysts and microreactors has achieved considerable progress [11]. Several structured systems based on CuO/CeO_2 using ceramic or metallic substrates have been analyzed [12–16]. In previous studies of our group, Co-ZrO_2, Co-CeO_2 and $MnCoCeO_x$ catalysts coated on cordierite monoliths were prepared and tested in CO preferential oxidation [17–19]. Redox properties were analyzed and correlated with physicochemical features of structured catalysts. Moreover, Ayastuy et al. [20] prepared CuO/CeO_2 catalysts with different copper loading, which were later washcoated over cordierite monoliths with the purpose of studying their performance in COPrOx. Recently, Lisi and coworkers [21,22] optimized the preparation of CuO/CeO_2 based monolithic reactors and studied the effect of substrate properties, slurry composition and preparation conditions. However, the design of a cordierite monolithic catalyst coated with CuO-CeO_2 dispersed in SBA-15 has never been explored in the open literature.

This work analyzes the influence of different variables that are key to achieve an active, stable monolithic catalyst based on CuO and CeO_2 over SBA-15 for the COPrOx reaction. In order to minimize the amount of the spent metal precursors, the CuO-CeO_2 active phase was dispersed in mesoporous silica. Firstly, one of the most significant factors studied to prepare the catalysts was the ratio between the CuO and CeO_2 active phases, their concentration and the method of incorporation into the mesoporous structure. Thus, powder catalysts with different CuO/CeO_2 ratios on SBA-15 were obtained so as to carry out preliminary activity studies and characterization of different formulations. Then, taking into account the advantages of structured catalysts for practical applications, CuO-CeO_2/SBA-15 solids were coated onto cordierite honeycomb monoliths to develop active, selective and stable monolithic catalysts.

The activity and selectivity of both structured and powder catalysts were evaluated for the preferential CO oxidation (COPrOx). The stability of selected catalysts was studied using both ultrasound tests (to evaluate the mechanical stability of the coatings) and time-on-stream experiments (in order to assess the catalytic stability of the best catalyst under reaction conditions). The effect of the addition of CO_2 and H_2O in the feed stream was also analyzed.

The monolithic catalysts were inspected by Scanning Electron Microscopy (SEM) to analyze the morphological characteristics of the precursor materials and the deposited films. Likewise, the mesoporous structure and the active phase were analyzed by Transmission Electron Microscopy (TEM) and Scanning Transmission Electron Microscope (STEM). Additionally, with the aim of identifying the nature of the active centers, monoliths and powder catalysts were also characterized by Temperature-Programmed Reduction (TPR), X-ray diffraction (XRD) and X-ray photoelectron spectroscopy (XPS).

Experimental

Preparation of powder and structured catalysts

Synthesis of SBA-15

SBA-15 mesoporous material was synthesized according to a previous method [23]. The solution was prepared with the following molar ratio: 1.0 TEOS:0.017 P123:5.6 HCl:197 H_2O. Pluronic P123 ($[(EO)_{20}(PO)_{70}(EO)_{20}]$, Aldrich) was used as the structure directing agent and tetraethylorthosilicate (TEOS, Aldrich) as the silica source. After stirring at 45 °C for 7.5 h the mixture was aged in an oven at 80 °C for 15.5 h. The product was recovered by filtration, washed with distilled water and dried. Finally, the material was calcined for 6 h at 550 °C in a muffle furnace to remove the surfactant from the pores.

CuO-CeO_2/SBA-15 catalysts

A series of catalysts with different CuO/CeO_2 molar ratios were prepared by the incipient wetness impregnation method over the SBA-15 support. Appropriate concentrations of precursor solutions, $Cu(NO_3)_2.3H_2O$ and/or $Ce(NO_3)_3.6H_2O$ in ethanol were added by successive impregnations or co-impregnation. In the first case, samples were impregnated with cerium nitrate, dried at 70–80 °C and, afterwards, copper nitrate was incorporated. The co-impregnation method consisted in a single step impregnation with a solution of both precursors. The obtained samples were denoted as CuCe-x, where "x" corresponds to the CuO/CeO_2 nominal molar ratio (Table 1) and "s" was added for those samples obtained by successive impregnations. Monometallic samples CuO/SBA-15 and CuO/SiO_2 were prepared by impregnation with copper nitrate (~5 wt. % CuO) on SBA-15 and SiO_2 (28 $m^2\ g^{-1}$), respectively. In addition, a bimetallic sample CuCe-0.55/SiO_2 was obtained by co-impregnation. All samples were dried overnight in an oven at 45 °C and then calcined at 450 °C for 6 h in air flow. The composition of the powders was measured by the Energy Dispersive X-ray Fluorescence technique, using an XRF spectrometer Shimadzu model EDX-720.

Table 1 – Chemical composition and textural properties of CuO-CeO_2/SBA-15 catalysts.

Catalysts[a]	CuO (wt. %)	CeO_2 (wt. %)	BET Specific surface area ($m^2 . g^{-1}$)	Total pore volume[b] ($cm^3 . g^{-1}$)	Average pore size[b] (nm)
CuCe-0.39	4.8[c] (4.4)	24.6[c] (24.3)	335	0.42	6.9
CuCe-0.39*	3.6 (3.4)	19.1 (18.9)	412	0.52	6.2
CuCe-0.55	4.9 (4.8)	19.1 (18.7)	430	0.52	6.2
CuCe-0.55s	5.2 (4.8)	19.0 (18.7)	410	0.50	6.2
CuCe-1.0	7.4 (7.2)	16.0 (15.7)	381	0.51	6.5
CuCe-2.2	10.3 (10.0)	9.9 (9.8)	313	0.45	6.7
CuCe-2.2s	10.4 (10.0)	9.8 (9.8)	345	0.48	6.5
SBA-15	–	–	650	0.70	7.0

* Lower concentration.
[a] CuCe-x powder catalysts, where x = CuO/CeO_2 molar ratio; (s) means successive impregnations.
[b] Calculated by BJH method.
[c] Actual concentrations determined by Energy Dispersive X-ray Fluorescence (EDX-RF) analysis. In brackets, nominal concentrations.

Structured catalysts

Honeycomb monoliths made of cordierite (Corning, 400 cpi, 0.1 mm wall thickness) were used as substrates. The cordierite composition was $2MgO\text{-}5SiO_2\text{-}2Al_2O_3$. The supports were cut in an average size of 1cm × 1cm × 1cm. As a cleaning procedure, cordierite pieces were washed in an ultrasonic bath (Testlab, 40 kHz and 160 W) with acetone for 30 min and then with distilled water. CuO-CeO_2/SBA-15 (CuCe-x) coatings were deposited onto cordierite by the washcoating technique, immersing the monoliths during 30 s in a CuCe-x slurry at room temperature. Slurries were prepared in distilled water (pH between 4 and 5) with solid concentrations between 10 and 20 wt. %, without binders or additives. The slurry viscosity was measured at room temperature using an RS 80 RheoStress HAAKE rheometer. During the washcoating, the pieces were blown with air for 10 s after each immersion to remove the slurry excess. Then, they were dried at 100 °C for 45 min. This immersion-blowing-drying cycle was repeated as many times as necessary to achieve the desired loading. Finally, the structured catalysts were calcined in air flow at 450 °C for 6 h. These samples were denoted as CuCe-xM, where "M" corresponds to structured catalysts and "x" indicates the CuO/CeO_2 molar ratio (Table 2).

Characterization techniques

Mechanical stability test

The mechanical stability test of the monolith coatings was performed to each structured catalyst previously calcined in order to evaluate the adherence of the catalytic coatings. The coated monoliths were immersed in petroleum ether inside a glass vessel, which was then placed in an ultrasonic bath during 10 min [24]. The samples were dried in an oven at 70 °C during 30–40 min. The sequence was repeated several times until the weight loss stayed stable. The weight was measured before and after each cycle.

Table 2 – Characteristics of structured CuO-CeO_2/SBA-15 catalysts.

Structured catalysts	Slurry concentration (wt. %)	Dips number	Total weight gained (wt. %)
CuCe-0.39M	15	9	31.3
CuCe-0.55M-20[a]	15	7	20.1
CuCe-0.55M-24[a]	20	8	23.8
CuCe-0.55M-30[a]	10	11	30.5
CuCe-1.0M	20	8	29.6
CuCe-2.2M	20	5	24.8

[a] Weight percentage of solid deposited on monolith walls.

Textural properties

The Brunauer-Emmet-Teller (BET) and Barrett–Joyner–Halenda (BJH) equations were used to calculate the specific surface area and average pore diameter of the materials from nitrogen adsorption and desorption isotherms, which were obtained at 77 K with an ASAP 2020 Micromeritics analyzer. Previously, the samples were degassed at 170–200 °C for 8 h. The total pore volume was measured at a relative pressure of 0.97.

Transmission Electron Microscopy (TEM)

Powder samples TEM images were recorded on an FEI® transmission electron microscope, Tecnai T20 model with an electron source of 200 kV. In addition, Scanning Transmission Electron Microscopy (STEM) images were obtained in high-angle annular dark-field (HAADF) mode using an FEI® transmission electron microscope (Tecnai F30 model) with an electron source of 300 kV, equipped with an XEDS system with a Li-drifted Si detector and an energy resolution of 130 eV.

Scanning Electron Microscopy (SEM) and Energy Dispersive Spectrometry (EDS)

With the objective of studying their morphology, SBA-15 powder and coatings of the monolithic samples were examined with a scanning electron microscope Phenom ProX (SEM, operated at 15 kV). The elemental chemical analysis in the film was performed using a fully integrated EDS detector and software of the mentioned microscope.

X-ray diffraction (XRD)

X-Ray diffraction peaks of powder samples were measured on a Shimadzu XD-D1 diffractometer with monochromator using a Cu-Kα radiation at a scanning rate of $2^\circ \cdot min^{-1}$ in $2\theta = 10–70^\circ$. The peaks observed for the catalysts were compared to standards published by JCPDS data (Joint

Committee on Powder Diffraction Standards). The crystallite size was estimated by Scherrer's equation.

The 2D ordered hexagonal structure of mesoporous materials was verified by low angle X-ray diffraction. The patterns were recorded on a Panalytical, X'Pert Celerator, (50 kV voltage), using a Cu Kα (λ = 1.5406 Å) as the X-ray source. The signal was recorded for 2θ = 0.5–3° with a step of 0.02°·s^{-1}. The d-spacing (100) and the unit-cell parameter a_0 were calculated from the basic equation of the Bragg law (λ/2·sen θ and $2 \cdot d_{100}/\sqrt{3}$ respectively).

Temperature programmed reduction (TPR)

The TPR analyses were carried out using 50 mg of powder samples. In the case of monolithic catalysts, they were finely milled in an agate mortar. A Micromeritics® analyzer, AutoChem 2950 HP model was used. Prior to the TPR measurements, the calcined solids were pretreated in argon heating up to 150 °C during 30 min. The reduction was performed using a 5% H_2/Ar mixture, with a 10 °C·min^{-1} ramp up to 900 °C.

X-ray photoelectron spectroscopy (XPS)

XPS analyses were carried out in a multi-technique system (SPECS) equipped with a dual Mg/Al X-ray source and a hemispherical PHOIBOS 150 analyzer operating in the fixed analyzer transmission (FAT) mode. The spectra were obtained with a pass energy of 30 eV, the Al Kα X-ray source (hυ = 1486.6 eV) was operated at 200 W and 12 kV. The working pressure in the analyzing chamber was less than 2 × 10^{-6} Pa. The XPS measurements of powder and monolithic catalysts were performed. Casa XPS software was employed for data treatment corresponding to regions Cu 2p, O 1s, Ce 3d, and Si 2p (as internal reference 103.4 eV). Peaks were considered as a mixture of Gaussian and Lorentzian functions in a 70/30 ratio.

Catalytic performance

Preferential CO oxidation experiments were performed in a fixed-bed flow reactor at atmospheric pressure. Powder and structured samples were placed in a tubular quartz reactor (15.6 mm i.d.). The reaction mixture consisted of CO 1 vol %, O_2 1 vol % and H_2 40 vol %, He balance, with a total gas flow 87 mL min^{-1} (STP). For each experiment, 0.2 g of catalyst were loaded into the reactor. Catalytic tests were run at a fixed contact time, τ = 0.138 g_{cat}·s·mL^{-1}(STP), g_{cat} being the catalyst weight. The mass of the cordierite substrate is excluded in the monolithic catalysts.

The effect of the addition of CO_2 (10 vol %) and H_2O (10 vol %) in the feed stream upon the catalytic behavior was studied for the most active structured catalyst.

The stability of the most active monolithic catalyst was studied by time-on-stream run performed during 80 h at 185 °C under reaction conditions.

The CO conversion was calculated from the change in CO concentration between the inlet and outlet gas streams (Eq. (1)). The oxygen selectivity towards CO_2 was defined according to Eq. (2).

$$C_{CO}(\%) = \frac{[CO]^0 - [CO]}{[CO]^0} \times 100 \quad (1)$$

$$S_{CO_2}(\%) = 0.5 \times \frac{[CO]^0 - [CO]}{[O_2]^0 - [O_2]} \times 100 \quad (2)$$

where [CO] and [O_2] are reactor exit concentrations and [CO]^0, [O_2]^0 represent feed concentrations, which were measured using a gas chromatograph (GC-2014 Shimadzu) with a thermal conductivity detector (TCD) equipped with a 5A molecular sieve column.

For comparison of catalytic activity, the turnover frequency (TOF, s^{-1}) at 85 °C was calculated according to Eq. (3).

$$TOF = C_{CO} \times Fco \times m_{cat}/N \quad (3)$$

where F_{CO} = 3.89 x 10^{-5} mol min^{-1} is the CO molar rate in the feed, m_{cat} = 0.2 g, and N is the number of active centers, mol·g_{cat}^{-1} (calculated from TPR data).

Results and discussion

Catalysts preparation

CuCe-x powder catalysts were synthesized with different CuO/CeO_2 molar ratios (labeled x). Table 1 shows the compositions of the materials prepared by co-impregnation in order to obtain four nominal molar ratios: 0.39, 0.55, 1.0 and 2.2. In addition, catalysts with molar ratio 0.55 and 2.2 prepared by successive impregnations are also shown. It can be observed that as the molar ratio (x) increases, the copper oxide content increases and the ceria content decreases (Table 1). In order to analyze the effect of oxides loading, another catalyst (CuCe-0.39*) was prepared with the same molar ratio as CuCe-0.39 but with a lower weight percentage of both oxides. The concentration values obtained by elemental analysis are included in Table 1.

Structured catalysts were prepared by the washcoating technique, using an aqueous suspension of the previously obtained materials (see Table 2). In order to inspect the influence of the above mentioned washcoating conditions upon the covering characteristics, monoliths with different catalyst content, between 20 and 31 wt. %, were prepared by combining different suspension concentrations and a number of immersions. The slurry concentration was selected between 10 and 20 wt. %, with viscosity values of 2.0 and 4.1 mPa s, respectively. In general, the gained mass in the monoliths indicates that as the slurry concentration decreases, the number of needed dips increases. However, it is not recommended to use highly concentrated suspensions as they could occlude the monolith channels. From the reported data, it is possible to infer that there is a relation between the number of immersions, gained weight and slurry concentration. When the concentration values of 15 and 20 wt. % were used, 7 or 8 dips were necessary for CuCe-0.55M to obtain weight gains of 20 and 23.8%, respectively (Table 2). These values are in agreement with those reported by Zamaro et al. [25], who studied the effect of slurry concentration of different zeolites washcoated onto cordierite monoliths. Moreover, mechanical resistance tests showed good film adherence to the structure walls, presenting mass loss values between 8 and 12% for all monoliths.

Characterization of monoliths and powder catalysts

Textural properties

Table 1 presents the textural properties of powder catalysts prepared by the incipient wetness impregnation method. The N_2 sorption measurements showed isotherms type IV according to IUPAC classification (Fig. S1 supplementary information), with an H1 hysteresis loop, which reveals the ordered one-dimensional mesopores pattern. In the desorption branch, a two-step capillary evaporation was observed, which could be associated with pore-plugging by deposited oxide particles. In the same vein, pore size distribution curves showed a sharp peak centered between 6.2 and 6.9 nm, somewhat smaller compared to the pore size of SBA-15 (Table 1).

Both surface area and pore volume decreased after introducing copper and ceria oxides (Table 1). It can be observed that while CuCe-0.55 and CuCe-0.39* presented the highest values, in agreement with their lower active phase loading, the other catalysts showed a surface loss of around 45%. Moreover, the incorporation method of oxides, successive impregnation or co-impregnation, did not significantly influence the textural properties of catalysts.

TEM, STEM, SEM and EDS results

Fig. 1 (A, B) shows TEM images of the internal pore structure of the synthesized SBA-15. The hexagonal ordering and parallel channels show well-organized mesoporous materials. The average pore size measured was around 6.5 nm.

The STEM images (Fig. 1C–F) allow observing the size and location of the oxides nanoparticles impregnated within the SBA-15 structure. In this way, diffuse edge particles with sizes between 5 and 10 nm distributed homogeneously in the hexagonal network can also be observed.

STEM images 1C and 1D correspond to CuCe-0.55, and images 1E and 1F belong to CuCe-2.2. The EDS spectrum confirmed the presence of copper, cerium and silicon (insets in Fig. 1C). In addition, it can be observed that the characteristic mesoporous structure for all CuCe-x catalysts was preserved. From these images, the pore diameter was estimated about 6–6.5 nm, in agreement with the values obtained from N_2 sorption experiments.

The SEM images show the SBA-15 powder and the monolith washcoated with the CuCe-0.55 powder (Fig. 2A and B). For the SBA-15 and CuCe-x catalysts, a common morphology was observed, fiber-like aggregates of 10–20 μm length and up to 5 μm thickness. Likewise, the size and the morphology of the monolithic catalysts remained similar to the parent material.

The top section view of the monolithic catalyst (Fig. 2B) exhibits apparently continuous layers since the macroporosity of the cordierite is completely covered. The layer composition was analyzed by EDS; Cu/Ce molar ratios of 0.57 and 2.33 were obtained for CuCe-0.55M and CuCe-2.2M, respectively. Furthermore, a layer thickness above 30 μm without cracks or fractures can be seen. The cross-section view (Fig. 2C) shows a thicker layer at the corners of the square cells caused by the fluid-dynamic phenomena during the blowing step of the deposition procedure.

Finally, Fig. 2D includes the linear scan of the elements present in the cross-section of the structured catalyst by the EDS technique. In the catalytic film, a high silicon concentration and low Cu and Ce concentrations were detected, in agreement with the catalytic formulation. On the other hand, the Mg and Al concentrations were constant in the cordierite wall and showed an abrupt decrease when reaching the film. If the silicon distribution is followed, the gradual concentration decrease from the interface (catalytic film-cordierite) to inside the wall can be observed. The interaction between the silica support with cordierite macropores enhanced the adherence of catalytic film.

XRD analysis

The mesoporous structural building of different CuCe-x catalysts and the SBA-15 support were analyzed by low angle X-ray diffraction (Fig. 3A). The main peak at 0.96° and two less intense peaks located at 1.64 and 1.88° corresponding to (100), (110) and (200) reflections of the 2D hexagonal phase confirmed the mesoporous arrangement of the SBA-15 structure [26]. A slight shift toward higher 2 theta values, observed in CuCe-0.55 (powder and monolith) and CuCe-2.2, revealed smaller lattice parameters (insets in Fig. 3A). The unit-cell parameter a_0 decreased from 10.5 nm to 10.2 nm and the d-spacing (100) from 9.1 to 8.8 nm for SBA-15 and CuCe-x catalyst, respectively. Moreover, the peaks intensity diminished if compared to the mesoporous support (not shown) due to the presence of oxides nanoparticles inside the channels.

In Fig. 3B, the CuCe-x catalysts show patterns dominated by the CeO_2 diffraction peaks. The main peaks appear at 2 theta 28.58, 33.11, 47.52, 56.38° (JCPDS N° 34-0394) corresponding to the fluorite phase. Moreover, a broad signal centered at 25°, belonging to the amorphous silica, can be observed. Only in CuCe-2.2s, two low intensity peaks at 2 theta 35.6° and 38.8° belonging to CuO phase were detected (not shown). In the other catalysts, the absence of copper species diffraction signals suggests that the particle size is not detectable by XRD due to the high dispersion on the silica surface. In this vein, Aguila et al. [6] reported that the simultaneous impregnation through Cu and Ce nitrates favored a high dispersion of CuO in the CuO-CeO_2/SiO_2 catalyst. In addition, there is no evidence of the formation of mixed oxide ($Ce_xCu_{1-x}O_2$). If the diffraction patterns of the CuCe-x catalysts are compared with CeO_2/SBA-15, there is no shift or widening of the ceria main peaks. The copper species do not seem to modify the structure of the CeO_2 diffraction pattern, so the copper species are not inserted in the lattice of the ceria.

Another factor that could improve the oxides dispersion on the silica mesoporous surface is the use of ethanol as a solvent during the impregnation. Tang et al. [8] showed that the wet impregnation with aqueous solutions of cerium and copper precursors worsen the COPrOx catalytic performance. On the other hand, Tao et al. [27] found a higher dispersion and stronger interactions of Ni metal particles with SBA-15 when ethanol was used as solvent instead of water during the impregnation method.

The average crystallite sizes estimated by Scherrer's equation from the (111) plane of CeO_2 phase were between 4.2 and 5.3 nm. The formation of nanometric particles smaller than 10 nm suggests a high dispersion of the oxides on the surface of the mesoporous material, which was confirmed by TEM-STEM images. Likewise, CeO_2 crystallite sizes estimated

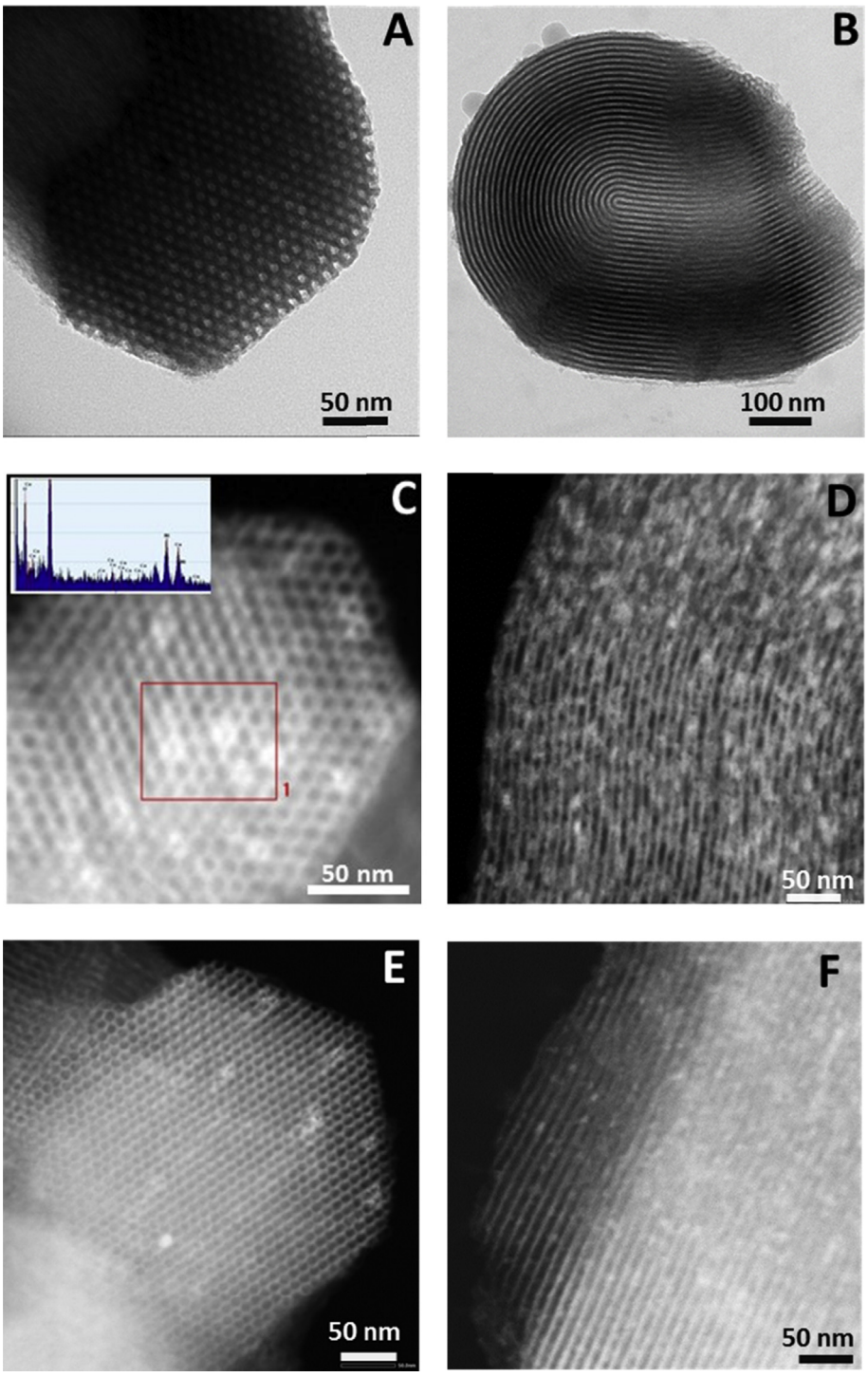

Fig. 1 – (A,B) TEM images of SBA-15. (C,D) and (E,F) HADDF-STEM images of CuCe-0.55 and CuCe-2.2 respectively. (A), (C) and (E) along the pore channel direction, (B), (D) and (F) direction perpendicular to the mesopore channel. The lower insert in (C) is EDS spectrum of area 1.

from the diffractograms are in the same order of magnitude as the sizes observed in the micrographs.

When the monolithic catalysts were measured by XRD, overlapping diffraction patterns were detected corresponding to the different phases present. It was possible to detect the dominant phase of CeO_2 and small signals (at 15.1° and 21.8°) of constituent oxides of cordierite (Fig. 3B).

TPR analysis

The temperature-programmed reduction study was carried out to elucidate the impact of the mesoporous support or active phase composition (CuO/CeO_2 ratio) on the redox properties of catalysts. Fig. 4 depicts the reduction profiles of catalysts in terms of hydrogen uptake as a function of temperature. Table 3 summarizes the amount of H_2 consumed up

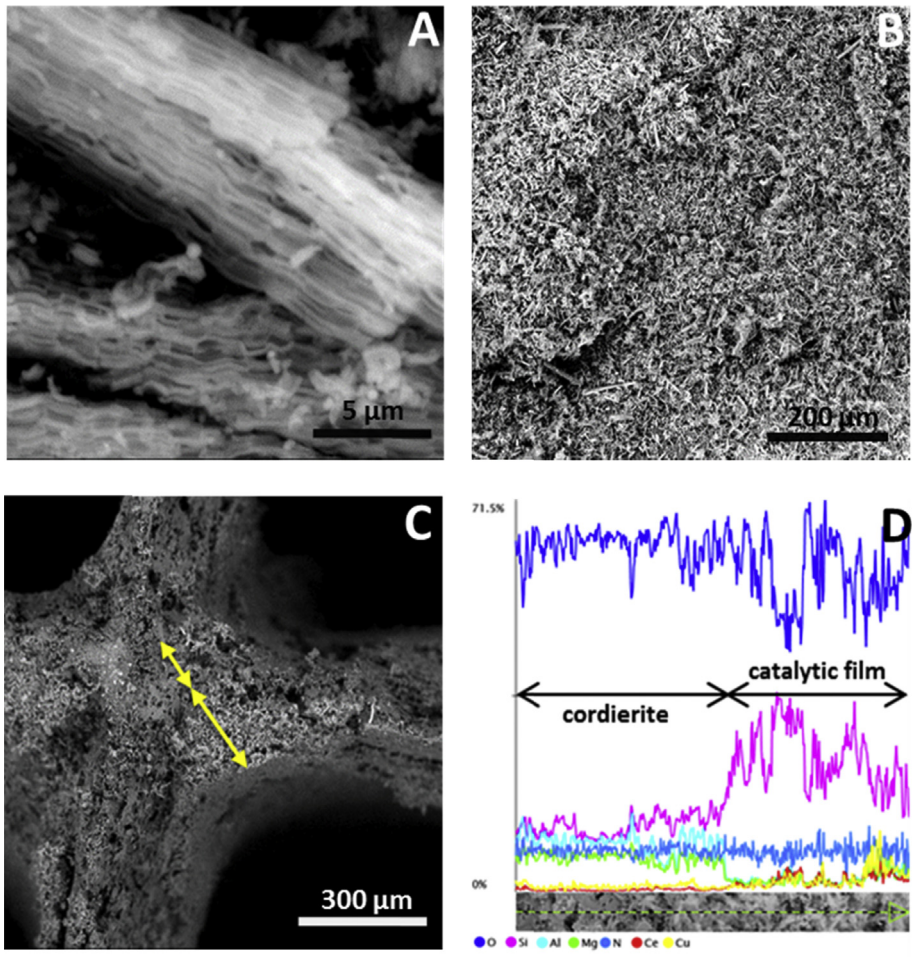

Fig. 2 – SEM images. (A) SBA-15 powder. (B,C) Structured catalyst CuCe-0.55M, top view and cross-section. (D) EDS linear scan over the line drawn in (C).

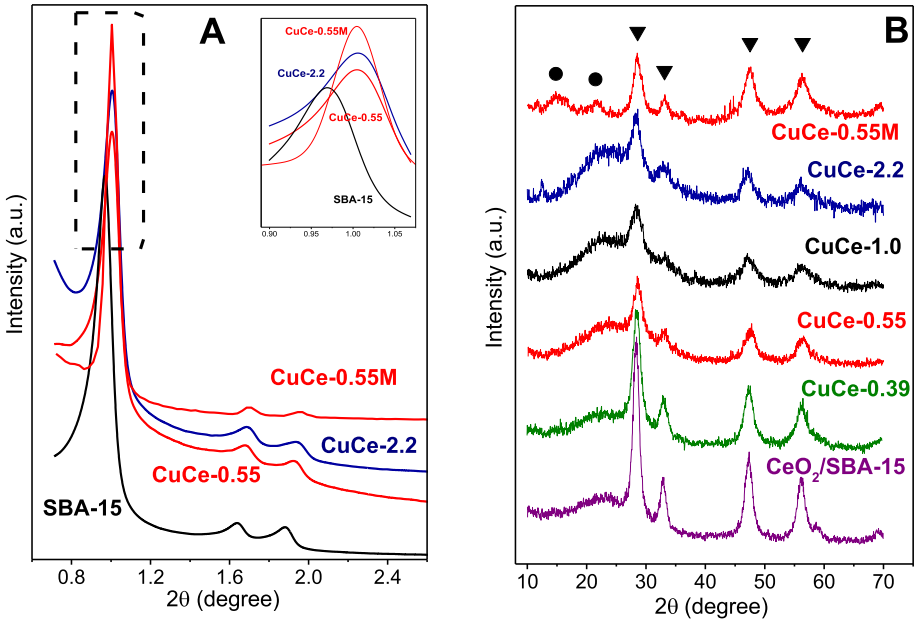

Fig. 3 – (A) Low angle XRD of SBA-15, CuCe-0.55, CuCe-2.2 and CuCe-0.55M samples. (B) High angle XRD of CeO_2/SBA-15, CuCe-0.39, CuCe-0.55, CuCe-1.0, CuCe-2.2 and CuCe-0.55M catalysts (▼ CeO_2, ● cordierite).

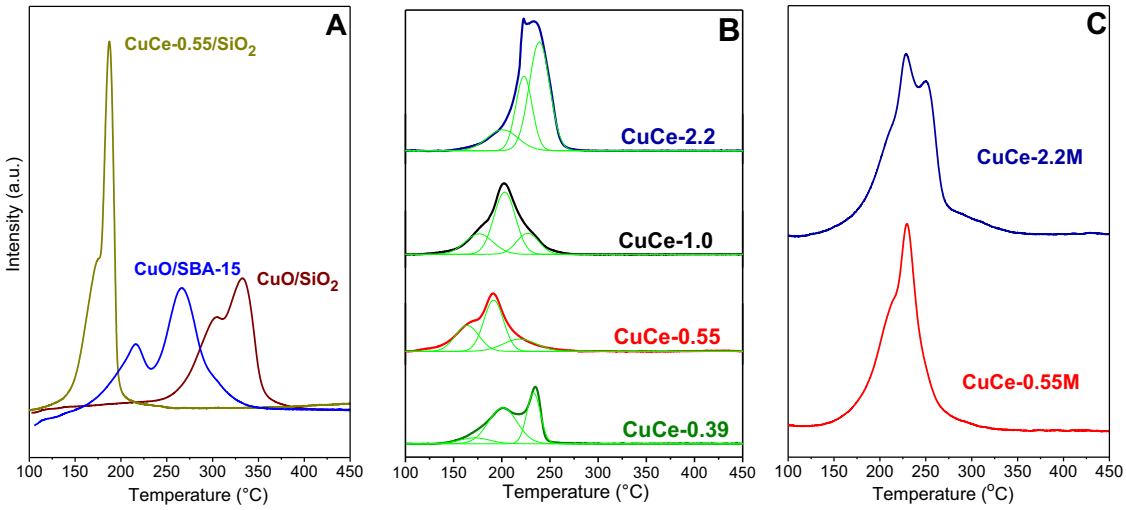

Fig. 4 – Reducibility of samples measured by temperature programmed reduction. (A) References samples. (B) CuCe-x catalysts. (C) CuCe-xM monolithic catalysts.

Table 3 – Temperature programmed reduction and turnover frequency.

Catalysts	CuO mmol/g	H_2 uptake[a] mmol/g		H_2/CuO molar ratio	TOF[d] ($x10^{-4}$ s^{-1})
		<225 °C	>225 °C		
CuCe-0.39	0.603	0.47	0.22	1.14	6.17
CuCe-0.55	0.616	0.63	0.15	1.27	10.0
CuCe-0.55s	0.654	0.60	0.03	0.96	5.50
CuCe-1.0	0.930	0.75	0.18	1.00	2.17
CuCe-2.2	1.295	0.69	0.82	1.17	0.50
CuCe-2.2s	1.307	0.65	0.76	1.08	0.50
CuO/SBA-15[b]	0.691	0.23	0.42	0.95	1.33
CuO/SiO_2[c]	0.460	–	0.46	1.00	–
$CuCe-0.55/SiO_2$	0.603	0.60	–	0.99	–

[a] H_2 consumption between (25–225 °C) and (225–450 °C).
[b] 5.5 wt. % CuO/SBA-15.
[c] 5.0 wt. % CuO/SiO_2.
[d] Turnover frecuency (TOF) calculated at 85 °C, see Eq. (3).

to 450 °C. The results were analyzed taking into account the reduction profiles of monometallic copper as reference samples shown in Fig. 4A. Firstly, it can be seen that the reducibility of CuO increases when the specific surface area of the support is larger due to an increase of copper oxide dispersion. The incipient wetness impregnation of the mesoporous support with copper nitrate solution promotes the dispersion and the intimate contact between different phases. In this case, CuO/SBA-15 presents two peaks at 216 and 266 °C, whereas CuO/SiO_2 showed a main peak at 332 °C and a shoulder at 303 °C. In both samples, the cupric oxide was completely reduced to less than 450 °C (H_2/CuO ~ 1.0). The shift observed between both profiles means that a higher CuO dispersion exists on SBA-15 mesoporous support. According to the literature [28–30], a higher dispersion of CuO species will result in a lower reduction temperature. On the other hand, the reduction peak above 300 °C can be assigned to CuO bulk reduction. The CuO particles on the surface of the mesoporous material are more easily reduced than the bulk ones, so the peak at low temperature is attributed to the reduction of the highly-dispersed copper oxide species, while the peak at high temperature is attributed to the reduction of larger CuO particles. The absence of peaks above 400 °C suggests that no copper silicate species were formed according to the TPR results found by Szegedi et al. [31].

The increased ease for CuO reduction in the presence of ceria has been observed in $CuO-CeO_2$ systems by several authors [5–7,32]. Thus, by adding ceria to the CuO/SiO_2 reference sample (Fig. 4A) the reduction profile was shifted to lower temperatures (from 332 °C to 187 °C) and copper oxide was reduced completely below 225 °C (Table 3). As reported by previous studies, the small peak or shoulder at 175 °C and the main peak at 187 °C can be assigned to interfacial copper species in close contact with ceria [6,10].

On the other hand, the promoting effect of ceria could also be observed in CuCe-x catalysts, whose reduction profiles are shown in Fig. 4B. According to the literature ([7–9] and references therein), TPR profiles are composed of three overlapping peaks (denoted as α, β and γ) corresponding to three types of copper species. The reduction peak at low temperature (α peak) can be attributed to small and highly dispersed copper species in intimate contact with ceria. The second peak at moderate temperature (β peak) is assigned to bigger CuO particles in less contact with ceria and the reduction peak at high temperature (γ peak) is attributed to the reduction of CuO agglomerated on SBA-15 surface. Table 3 shows the H_2 consumption calculated in the low temperature range (25–225 °C) associated with (α+β) peaks and in the high temperature range (225–450 °C).

Fig. 4B depicts the reduction profile of the CuCe-0.39 catalyst, with peaks at 172 °C, 201 °C and 233 °C, aforementioned (α), (β) and (γ), respectively. The reduction profile of CuCe-0.55 shifted to lower temperatures with three overlapping peaks at 164 °C (α), 191 °C (β) and 220 °C (γ). Similarly, for the CuCe-1.0 catalyst, peaks at 176 °C, 203 °C and 227 °C can be observed.

For these catalysts, the H_2 consumption values (Table 3) indicate that more than 80% of copper is reduced below 225 °C. With higher CuO/CeO_2 molar ratio, the maximum temperatures increased and the CuCe-2.2 catalyst with 10 wt.% CuO showed peaks centered at 200 °C, 223 °C and 239 °C, respectively. In this catalyst, larger CuO particles on the SBA-15 surface were present. Instead, the catalyst prepared by successive impregnations (CuCe-2.2s) showed a similar profile with a H_2 consumption maximum at 181 °C, 203 °C and 229 °C (not shown).

In addition, it is possible to observe the ratio H_2/CuO is greater than 1, which suggests that the formation of metallic copper promotes the reduction of Ce^{+4} to Ce^{+3} species above 225 °C. From the H_2 uptake, it was possible to estimate the Ce^{+4} reduction extent, considering that the CuO present in the solid was completely reduced in the analyzed temperature range (Table 3). In this way, around 30% of Ce^{+4} were reduced in the CuCe-0.55 catalyst, but only 12% in CuCe-0.39 while for CuCe-0.55s and CuCe-1.0 the ceria was not reduced below 450 °C.

In addition, selected structured catalysts were studied by TPR. When the reduction profile of the CuCe-0.55M monolith was compared to its associated powder CuCe-0.55 (Fig. 4B and C), it was possible to observe a shift towards higher temperatures, with a peak at 230 °C and a shoulder at 210 °C. On the other hand, the reduction profiles of monolith and powder with $CuO/CeO_2 = 2.2$ were similar.

XPS results

By means of XPS, the electronic levels of Ce 3d and Cu 2p were measured to determine the oxidation state and their relative abundance on the surface of the catalysts (Table 4).

The complex Ce 3d spectrum of CuCe-0.55 catalyst was fitted with six component peaks (denominated v, v'' and v''' for Ce $3d_{5/2}$ and u, u'' and u''' for Ce $3d_{3/2}$) whose binding energy (BE) positions were very close to those found for the CeO_2 (Ce^{4+}) [33]. In the CuCe-0.55M monolith, after use under reaction conditions, four additional peaks were detected belonging to Ce^{3+}, which overlapped the Ce^{4+} peaks. These signals are coincident with those observed for the CuCe-0.55 catalyst reduced in situ by H_2/Ar at 170 °C (Table 4). According to XPS data, about 42% of surface cerium (4+) was reduced to Ce^{3+} during the COPrOx reaction.

On the other hand, the Cu 2p region showed a Cu $2p_{3/2}$ main peak at 933.4 eV corresponding to Cu^{2+} of CuO. A slight asymmetry observed on the left side of the peak suggests another component (at 935.1 eV) in lower concentration, which could be assigned to Cu species with strong interaction with the support [34]. The presence of Cu^{2+} species is sustained by a satellite peak at higher binding energies (942–943 eV). The monolithic used catalyst CuCe-0.55M showed the presence of Cu^{2+} species and another component at 932.5 eV corresponding to Cu^{1+} or Cu° components [10]. For CuCe-0.55 powder and monolith, the (Cu/Ce) molar surface ratios were 0.68 and 0.40 respectively, very close to the bulk value (0.55).

Catalytic performance in CO preferential oxidation

In order to study the effect of the CuO/CeO_2 ratio, the catalytic activity of several $CuO\text{-}CeO_2$/SBA-15 formulations prepared by successive or co-impregnations was tested. Powder catalysts obtained by co-impregnation with four molar ratios CuO/CeO_2 were evaluated for COPrOx, and the results are shown in Fig. 5. It can be seen that as temperature increased, the CO conversion increased until reaching a maximum value above 150 °C (Fig. 5A). The CuCe-x catalysts (except catalysts with $CuO/CeO_2 = 2.2$) showed CO conversion curves above those obtained for CuO/SBA-15. In this vein, when CuCe-0.39 (4.8 wt. % CuO plus 24.6 wt. % CeO_2) was tested, the maximum CO conversion achieved was 74% at 160 °C. In addition, the CuCe-0.39* catalyst with lower oxides content than the previous one (Table 1) was less active, with $X_{CO} = 64\%$ at 185 °C. The CuCe-0.55 formulation was the most active catalyst, reaching 100% CO conversion at 160 °C. It is possible to observe that the CO conversion curve was always higher than the other formulations throughout the temperature range studied (Fig. 5A).

On the other hand, catalysts with higher CuO/CeO_2 molar ratios (1.0 and 2.2) were less active, showing a moderate increase of conversion with temperature reaching values of 30–40% between 175 and 210 °C. The CO conversion was evaluated in the absence of H_2 (using the same contact time). The most active catalyst was the CuCe-1.0, reaching complete CO conversion at 175 °C (Fig. S2 supplementary information). CuCe-0.39 and CuCe-0.55 showed similar behaviors, with complete conversion above 200 °C. On the other hand, 95% CO conversion was obtained with CuCe-2.2 at 225 °C.

The O_2 selectivity towards CO_2 is displayed in Fig. 5B, in which it can be observed that the selectivity values decreased as the temperature increased. When the CO conversion was maximum, the selectivity was around 50–60% for the best

Table 4 – XPS results.

Catalysts	Binding Energies (fwhm)/eV		$Ce^{+3}/(Ce^{+3}+Ce^{+4})$	$Cu/Ce)_s$[c]
	Ce $3d_{5/2}$	$Cu2p_{3/2}$		
CuCe-0.55 calcined[a]	898.7 (3.0)	933.4(3.0) 935.1(3.5)	0.0	0.68
CuCe-0.55 reduced[b]	899.0 (4.0)	934.0 (3.5)	0.51	0.56
	886.0 (4.5)	933.0 (2.7)		
CuCe-0.55M used	898.6 (3.3)	934.0 (3.4)	0.42	0.40
	885.3 (3.8)	932.5 (2.6)		

[a] Powder catalyst calcined in air at 550 °C.
[b] Reduced catalyst at 170 °C under a 5% H_2/Ar stream.
[c] Surface atomic ratio, calculated considering Cu($2p_{3/2}$) and Ce($3d_{5/2}$).

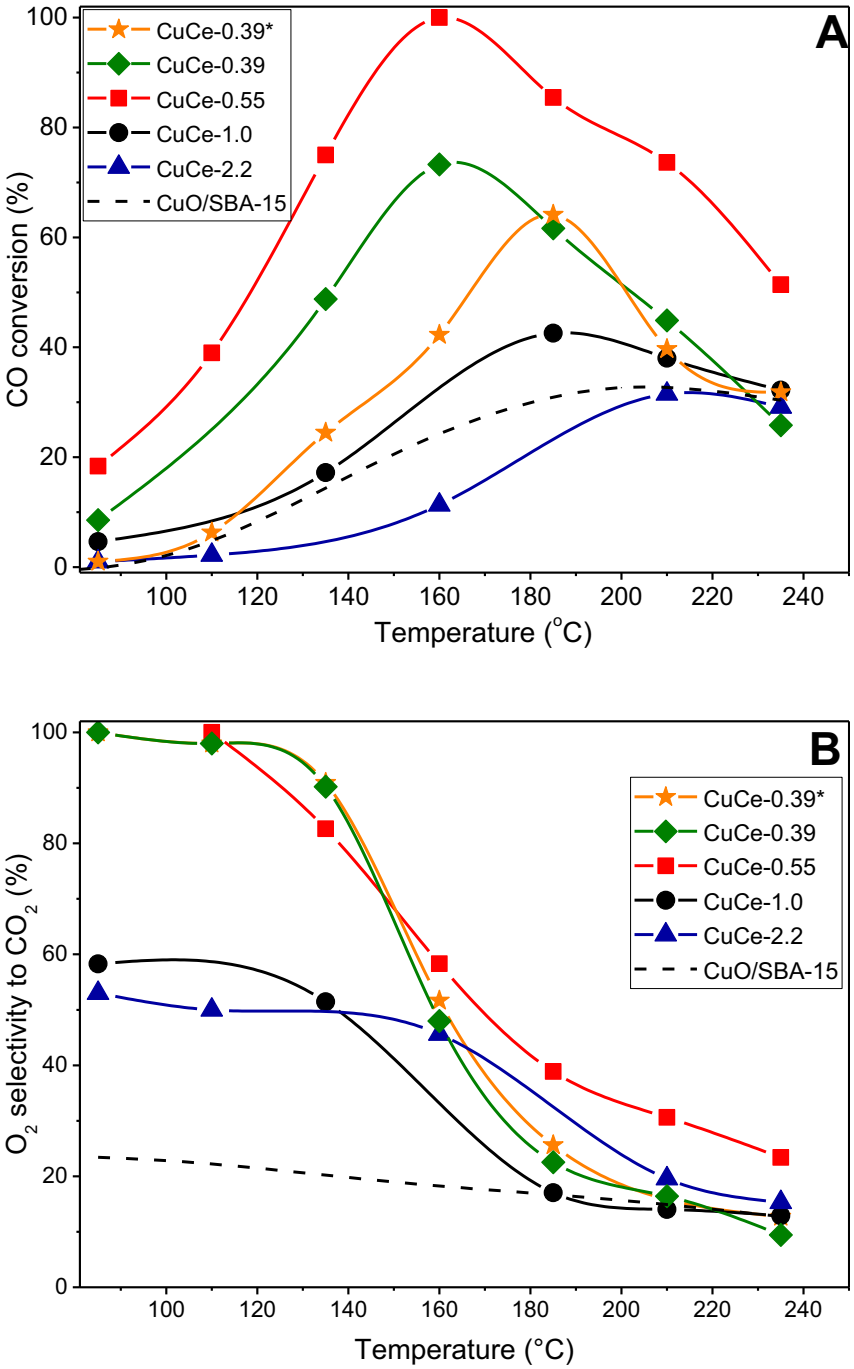

Fig. 5 – Catalytic performance of powder catalysts. (A) CO conversion, (B) Selectivity of O_2 to CO_2. Reaction conditions: 1% CO, 1% O_2, 40% H_2 in He balance. $\tau = 0.138\ g_{cat}{\cdot}s{\cdot}mL^{-1}$(STP).

catalysts. In those catalysts with lower ratios (0.39 and 0.55), the selectivity values resulted above 80% up to 150 °C.

The catalytic behavior of the two catalysts prepared by successive impregnations, with CuO/CeO_2 molar ratios of 0.55 and 2.2 respectively, were tested in order to study the influence of the impregnation method (Fig. S3 supplementary information). The CO conversion for CuCe-0.55s was better than CuCe-0.55; however, both catalysts reached 100% at 160 °C. On the other hand, the CuCe-2.2s catalyst showed low conversion and selectivity values similar to those of CuCe-2.2 prepared by co-impregnation.

It is well known that the $CuO\text{-}CeO_2$ system activity is correlated with the synergetic interactions between copper and ceria, which are dispersed in another support. In this vein, most authors agree that actives sites for the COPrOx reaction are related to interfacial copper oxide which is in intimate contact with ceria [6,8,35]. Moreover, it has been established that the COPrOx reaction path follows a redox mechanism

over CuO-CeO_2 catalysts, involving the change in oxidation state of both copper (Cu^{+2}/Cu^{+1}) and cerium (Ce^{+4}/Ce^{+3}).

According to the catalytic results of the CuCe-x powder catalysts reported in this work, the most active one contains 4.9 and 19.1 wt. % of CuO and CeO_2, respectively. It should be noted that a higher CO conversion and good O_2 selectivity at lower temperature were observed for the CuCe-0.55 catalyst. In this one, a suitable combination of CuO and CeO_2 nanoparticles (<5 nm) well dispersed on the support and sufficiently close to each other were identified by XRD and XPS. In consequence, the synergic effect promoted the oxides reducibility; thus, the redox cycle Cu^{2+}/Cu^{+1} and Ce^{3+}/Ce^{+4} occurred more easily. In this catalyst, the H_2 consumption measured by TPR evidenced that copper (+2) species were completely reduced below 225 °C (α+β peaks), which promoted the reduction of ceria. The CO conversion decreased with copper concentrations above 7 wt. % (CuCe-1.0 and CuCe-2.2 catalysts) where the copper reducibility was lower. The ceria promoted effect was less significant in CuCe-2.2, with a high concentration of cupric oxide (10 wt. %) and the lowest content of ceria (9.8 wt. %). The reduction temperature above 200 °C suggests an increase in the particle size of the oxides which impacted on catalytic activity, CuCe-2.2 and CuCe-2.2s being the worst catalysts. Thus, it is possible to propose that there is an optimal ratio of CuO/CeO_2 close to 0.55 within the range (0.39–2.2) which maximizes the CO conversion to the lowest temperature. In addition, it is necessary to achieve an appropriate concentration of active sites, since with the same ratio (0.39* vs. 0.39) a higher concentration of oxides improves CO conversion without changing the selectivity curve to CO_2 (Fig. 5). In order to compare the activity of catalysts, the TOF values at 85 °C were estimated (Table 3), the higher values being obtained for CuCe-0.55 and CuCe-0.39 catalysts, where a suitable relative concentration between CuO and CeO_2 phases improved the redox activity among them.

Fig. 6 shows the results of CO conversion and O_2 selectivity towards CO_2 over the monolithic catalysts. During the tests, the same *catalytic mass/total flow* ratio as powders was used (GHSV = 6500 h^{-1}, calculated by using monolith void volume). Fig. 6A shows an improvement in catalytic activity when the solids were supported on the monolith for CuCe-1.0M and CuCe-2.2M. The CO conversion values significantly increased for CuCe-2.2M, where the maximum CO conversion was 74% at 200 °C, more than twice that of the corresponding powder sample.

Meanwhile, the most active and selective monolith, CuCe-0.55M – 24, reached almost 85% CO conversion and S = 48% at 185 °C. The O_2 selectivity was higher for all monoliths up to 200 °C compared with their respective powders (compare Fig. 6B with Fig. 5B). From TPR results, it can be noted that copper reducibility decreased with the main peak above 225 °C (Fig. 4C). The activity of the CuCe-2.2M monolithic catalyst was tested at higher temperatures after reaching the maximum. CO conversion decreased to 48% at 225 °C, higher than that of CuCe-0.55M and CuCe-1.0M (Fig. 6A).

At this point, we consider that by incorporating the active phase film over the monolith walls, new factors appear which affect the catalytic activity. These factors are related to the slurry concentration, pH of the aqueous medium and particles size of suspension among others, which will be investigated more deeply.

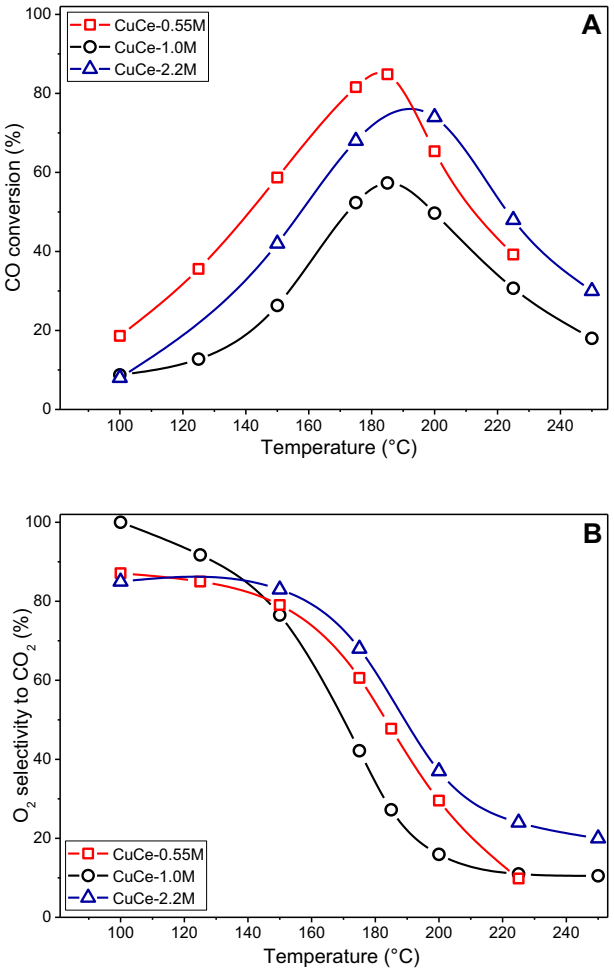

Fig. 6 – Catalytic performance of structured catalysts. (A) CO conversion, (B) Selectivity of O_2 to CO_2. Reaction conditions: 1% CO, 1% O_2, 40% H_2 in He balance. τ = 0.138 g_{cat}·s·mL^{-1}(STP).

The addition of 10% CO_2 in the feed caused a slight shift to lower conversions over the CuCe-0.55M catalyst (Fig. 7A). Moreover, the simultaneous addition of 10% CO_2 and 10% H_2O deactivated the catalyst shifting the CO conversion curve to higher temperatures, with a maximum conversion X_{CO} = 62% at 200 °C. From previous studies, this phenomenon was explained by the competitive adsorption of CO and CO_2 and the blocking effect of water [5,21,36]. On the other hand, from 185 °C, the selectivity was improved in the presence of CO_2 and H_2O, indicating that these two compounds inhibit both CO and H_2 oxidation (Fig. 7B).

The long term stability of CuCe-0.55M was evaluated at 185 °C under reaction conditions with the addition of 10% CO_2 and 10% H_2O (Fig. 8). When 10% CO_2 was added to the feed, a slight drop in conversion and selectivity was observed. However, the activity was stable during 64 h of time-on-stream and no sign of deactivation could be detected after several hours on stream. A similar behavior was found in CuO/CeO_2 catalysts by Di Benedetto et al. [37]. They showed that the

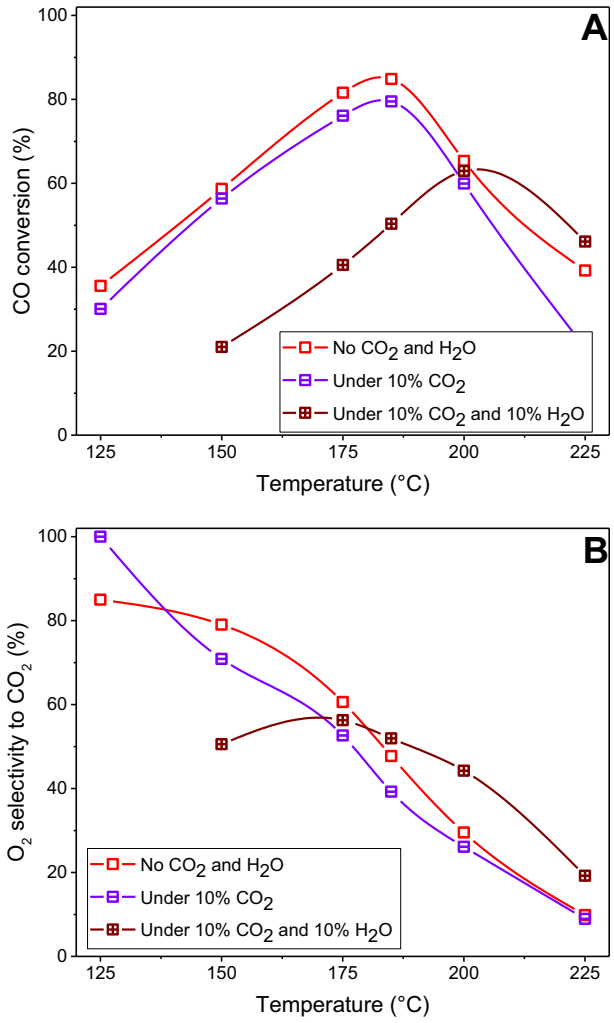

Fig. 7 – Effect of CO_2 and H_2O addition on catalytic performance of CuCe-0.55M. (A) CO conversion, (B) Selectivity of O_2 to CO_2. Reaction conditions: 1% CO, 1% O_2, 40% H_2, 10% CO_2 and 10% H_2O, in He balance. $\tau = 0.138$ $g_{cat}{\cdot}s{\cdot}mL^{-1}$(STP).

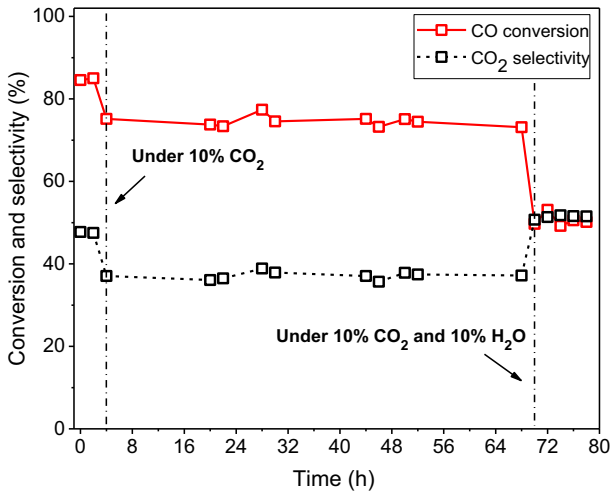

Fig. 8 – Long-term stability test for COPrOx on CuCe-0.55M at 185 °C. Reaction conditions: 1% CO, 1% O_2, 40% H_2, 10% CO_2 and 10% H_2O, in He balance. $\tau = 0.138$ $g_{cat}{\cdot}s{\cdot}mL^{-1}$(STP).

catalyst was stable and that no continuous accumulation of any species (hydroxyls or carbonates) occurred during the reaction with CO_2 added in the feed. After 70 h under reaction conditions (Fig. 8), the addition of 10% H_2O and 10% CO_2 provoked a partial deactivation, since the CO conversion dropped to 50%, the selectivity increased to 53% and both remained constant during 8 h.

A straightforward performance comparison of our catalysts with those reported in the literature is complex, due to the different active phases used and the reaction conditions selected, especially if it is taken into account that the active phase CuO-CeO_2 was dispersed in the mesoporous support and then deposited over the monolith walls. Catalytic results of previous studies in Cu-Ce supported generally showed an optimal copper concentration, above which no improvement in activity was observed. Among our catalysts, the most active one was CuCe-0.55, where the CO conversion was higher than 90% between 145 and 180 °C (contact time $\tau = 0.138$ $g_{cat}{\cdot}s{\cdot}mL^{-1}$). For instance Cecilia et al. [9] reported CO conversion values close to 100% at 115 °C with CuO-CeO_2 supported on porous clay ($CuO/CeO_2 = 0.66$, $\tau = 0.18$ $g_{cat}{\cdot}s{\cdot}cm^{-3}$). CuO-$CeO_2$/SBA-15 catalysts prepared by solid state impregnation [8] displayed an operation window with more than 99% CO conversion between 120 and 180 °C for $CuO/CeO_2 = 0.54$ ($\tau = 0.2$ $g_{cat}{\cdot}s{\cdot}cm^{-3}$). They found that the absence of solvent during impregnation improved the interaction between copper and ceria.

In previous papers, copper/ceria (without silica support) whascoated on different structured systems have been studied as COPrOx catalysts. In this respect, Landi et al. [22] reported around 100% CO conversion above 130 °C with 80% selectivity (GHSV = 27,000 h^{-1}) with CuO-CeO_2 on cordierite monolith. Likewise, Gu et al. [38] prepared CuO-CeO_2 on meso-macroporous alumina monoliths and reached CO conversions above 90% between 145 and 205 °C at GHSV = 10,000 h^{-1}.

Finally, it can be said that the incorporation of active phases into the structured support generally produces better catalysts, improving the O_2 selectivity and the CO conversion. Nevertheless, most studies concerning CO preferential oxidation have been performed using powder catalysts, but it is recognized that structured catalysts are necessary in this type of reactions for practical applications.

Conclusions

Powders and monolithic catalysts based on CuO-CeO_2/SBA-15 were synthesized with different CuO/CeO_2 ratios and tested on the CO preferential oxidation reaction in H_2-rich streams.

Well-dispersed nanoparticles of CuO and CeO_2 within SBA-15 pores were obtained using successive or co-impregnation with a dissolution of precursors in ethanol. The CuO/CeO_2 molar ratio (x), concentration and dispersion of active phase showed a marked influence on the catalytic activity.

For monolithic and powder catalysts, it was possible to find that x = 0.55 was the optimum value in the range from 0.39 to

2.2 since 100% CO conversion at 160 °C was reached in CuCe-0.55.

The active sites of the COPrOx reaction were related to the interfacial copper oxide in intimate contact with ceria, which was favored by oxide particles of nanometric order (<10 nm). In addition, the TPR results revealed that SBA-15 support allowed the dispersion and reducibility (at low temperature) of CuO and CeO_2 phases and consequently improved the exchange of the redox couple involved in the COPrOx reaction.

All monoliths showed a homogeneous and mechanically stable catalytic film composed of fiber-like aggregates, whose original morphology was preserved. The layers that covered or filled the macropores of cordierite walls conferred mechanical stability to catalysts. The catalyst deposition on the monolithic walls improved the catalytic performance of CuCe-1.0M and CuCe-2.2M.

Preliminary catalytic evaluations were carried out with the best monolithic catalyst CuCe-0.55M and they revealed that the CO conversion decreased from 85% to 75% with the addition of 10% CO_2 in the feed and remained constant during 64 h at 185 °C, due to competitive adsorption of CO and CO_2. Likewise, the addition of 10% H_2O caused a drop in CO conversion to 50%. The presence of CO_2 and H_2O in the feed stream partially deactivated the catalysts, blocking the active sites for CO adsorption in the reaction path.

Acknowledgments

The authors wish to acknowledge the financial support received from UNL, ANPCyT, and CONICET. They are also grateful to ANPCyT for PME Grants to finance the purchase of characterization equipment. Thanks are given to María Fernanda Mori for the XPS measurements.

Appendix A. Supplementary data

Supplementary data related to this article can be found at https://doi.org/10.1016/j.ijhydene.2018.05.122.

REFERENCES

[1] Liu K, Wang A, Zhang T. Recent advances in preferential oxidation of CO reaction over platinum group metal catalysts. ACS Catal 2012;2:1165–78. https://doi.org/10.1021/cs200418w.

[2] Konsolakis M. The role of Copper–Ceria interactions in catalysis science: recent theoretical and experimental advances. Appl Catal B Environ 2016;198:49–66. https://doi.org/10.1016/j.apcatb.2016.05.037.

[3] Guo X, Mao J, Zhou R. Influence of the copper coverage on the dispersion of copper oxide and the catalytic performance of CuO/CeO_2(rod) catalysts in preferential oxidation of CO in excess hydrogen. J Power Sources 2017;371:119–28. https://doi.org/10.1016/j.jpowsour.2017.10.055.

[4] Wang, Pu H, Wan G, Chen K, Lu J, Lei Y, et al. Promoted the reduction of Cu^{2+} to enhance $CuO-CeO_2$ catalysts for CO preferential oxidation in H_2-rich streams: effects of preparation methods and copper precursors. Int J Hydrogen Energy 2017;42:21955–68. https://doi.org/10.1016/j.ijhydene.2017.07.122.

[5] Jampa S, Wangkawee K, Tantisriyanurak S, Changpradit J, Jamieson AM, Chaisuwan T, et al. High performance and stability of copper loading on mesoporous ceria catalyst for preferential oxidation of CO in presence of excess of hydrogen. Int J Hydrogen Energy 2017;42:5537–48. https://doi.org/10.1016/j.ijhydene.2016.08.078.

[6] Águila G, Gracia F, Araya P. CuO and CeO_2 catalysts supported on Al_2O_3, ZrO_2, and SiO_2 in the oxidation of CO at low temperature. Appl Catal A Gen 2008;343:16–24. https://doi.org/10.1016/j.apcata.2008.03.015.

[7] Astudillo J, Águila G, Díaz F, Guerrero S, Araya P. Study of $CuO–CeO_2$ catalysts supported on SiO_2 on the low-temperature oxidation of CO. Appl Catal A Gen 2010;381:169–76. https://doi.org/10.1016/j.apcata.2010.04.004.

[8] Tang C, Sun J, Yao X, Cao Y, Liu L, Ge C, et al. Efficient fabrication of active $CuO-CeO_2$/SBA-15 catalysts for preferential oxidation of CO by solid state impregnation. Appl Catal B Environ 2014;146:201–12. https://doi.org/10.1016/j.apcatb.2013.05.060.

[9] Cecilia JA, Arango-Díaz A, Franco F, Jiménez-Jiménez J, Storaro L, Moretti E, et al. $CuO-CeO_2$ supported on montmorillonite-derived porous clay heterostructures (PCH) for preferential CO oxidation in H_2-rich stream. Catal Today 2015;253:126–36. https://doi.org/10.1016/j.cattod.2015.01.040.

[10] Reyes-Carmona Á, Arango-Díaz A, Moretti E, Talon A, Storaro L, Lenarda M, et al. CuO/CeO_2 supported on Zr doped SBA-15 as catalysts for preferential CO oxidation (CO-PROX). J Power Sources 2011;196:4382–7. https://doi.org/10.1016/j.jpowsour.2010.10.019.

[11] Laguna OH, Domínguez MI, Centeno MA, Odriozola JA. Catalysts on metallic surfaces: monoliths and microreactors. In: Parvulescu VI, Kemnitz E, editors. New Materials for Catalytic Applications, Amsterdam; 2016. p. 81–120. https://doi.org/10.1016/B978-0-444-63587-7.00004-4.

[12] Zeng SH, Liu Y, Wang YQ. $CuO-CeO_2/Al_2O_3$/FeCrAl monolithic catalysts prepared by sol-pyrolysis method for preferential oxidation of carbon monoxide. Catal Lett 2007;117:119–25. https://doi.org/10.1007/s10562-007-9116-7.

[13] Gu X, Li H, Liu L, Tang C, Gao F, Dong L. Promotional effect of CO pretreatment on CuO/CeO_2 catalyst for catalytic reduction of NO by CO. J Rare Earths 2014;32:139–45. https://doi.org/10.1016/S1002-0721(14)60043-0.

[14] Pennemann H, Kolb G. Review: microstructured reactors as efficient tool for the operation of selective oxidation reactions. Catal Today 2016;278:3–21. https://doi.org/10.1016/j.cattod.2016.04.032.

[15] Laguna OH, González Castaño M, Centeno MA, Odriozola JA. Microreactors technology for hydrogen purification: effect of the catalytic layer thickness on CuO_x/CeO_2-coated microchannel reactors for the PROX reaction. Chem Eng J 2015;275:45–52. https://doi.org/10.1016/j.cej.2015.04.023.

[16] Jing G, Zhang X, Zhang A, Li M, Zeng S, Xu C, et al. CeO_2-CuO/Cu_2O/Cu monolithic catalysts with three-kind morphologies Cu_2O layers for preferential CO oxidation. Appl Surf Sci 2018;434:445–51. https://doi.org/10.1016/j.apsusc.2017.10.212.

[17] Gómez LE, Tiscornia IS, Boix AV, Miró EE. Co/ZrO_2 catalysts coated on cordierite monoliths for CO preferential oxidation. Appl Catal A Gen 2011;401:124–33. https://doi.org/10.1016/j.apcata.2011.05.007.

[18] Gómez LE, Tiscornia IS, Boix AV, Miró EE. CO preferential oxidation on cordierite monoliths coated with Co/CeO_2 catalysts. Int J Hydrogen Energy 2012;37:14812–9. https://doi.org/10.1016/j.ijhydene.2012.01.159.

[19] Gómez LE, Boix AV, Miró EE. Co/ZrO_2, Co/CeO_2 and MnCoCe structured catalysts for COPrOx. Catal Today 2013;216:246–53. https://doi.org/10.1016/j.cattod.2013.05.010.

[20] Ayastuy JL, Gamboa NK, González-Marcos MP, Gutiérrez-Ortiz MA. CuO/CeO_2 washcoated ceramic monoliths for CO-PROX reaction. Chem Eng J 2011;171:224–31. https://doi.org/10.1016/j.cej.2011.03.006.
[21] Barbato PS, Di Benedetto A, Landi G, Lisi L. CuO/CeO_2 based monoliths for CO preferential oxidation in H_2-rich streams. Chem Eng J 2015;279:983–93. https://doi.org/10.1016/j.cej.2015.05.079.
[22] Landi G, Barbato PS, Di Benedetto A, Lisi L. Optimization of the preparation method of CuO/CeO_2 structured catalytic monolith for CO preferential oxidation in H_2-rich streams. Appl Catal B Environ 2016;181:727–37. https://doi.org/10.1016/j.apcatb.2015.08.040.
[23] Meynen V, Cool P, Vansant EF. Verified syntheses of mesoporous materials. Microporous Mesoporous Mater 2009;125:170–223. https://doi.org/10.1016/j.micromeso.2009.03.046.
[24] Pérez H, Navarro P, Montes M. Deposition of SBA-15 layers on Fecralloy monoliths by washcoating. Chem Eng J 2010;158:325–32. https://doi.org/10.1016/j.cej.2010.01.032.
[25] Zamaro JM, Ulla MA, Miró EE. The effect of different slurry compositions and solvents upon the properties of ZSM5-washcoated cordierite honeycombs for the SCR of NO_x with methane. Catal Today 2005;107–108:86–93. https://doi.org/10.1016/j.cattod.2005.07.066.
[26] Zhao D. Triblock copolymer syntheses of mesoporous silica with periodic 50 to 300 angstrom pores. Science (80-) 1998;279:548–52. https://doi.org/10.1126/science.279.5350.548.
[27] Tao M, Meng X, Lv Y, Bian Z, Xin Z. Effect of impregnation solvent on Ni dispersion and catalytic properties of Ni/SBA-15 for CO methanation reaction. Fuel 2016;165:289–97. https://doi.org/10.1016/j.fuel.2015.10.023.
[28] Tu CH, Wang AQ, Zheng MY, Wang XD, Zhang T. Factors influencing the catalytic activity of SBA-15-supported copper nanoparticles in CO oxidation. Appl Catal A Gen 2006;297:40–7. https://doi.org/10.1016/j.apcata.2005.08.035.
[29] Patel A, Shukla P, Rufford T, Wang S, Chen J, Rudolph V, et al. Catalytic reduction of NO by CO over copper-oxide supported mesoporous silica. Appl Catal A Gen 2011;409–410:55–65. https://doi.org/10.1016/j.apcata.2011.09.024.
[30] Yang JS, Jung WY, Lee GD, Park SS, Jeong ED, Kim HG, et al. Catalytic combustion of benzene over metal oxides supported on SBA-15. J Ind Eng Chem 2008;14:779–84. https://doi.org/10.1016/j.jiec.2008.05.008.
[31] Szegedi Á, Popova M, Lázár K, Klébert S, Drotár E. Impact of silica structure of copper and iron-containing SBA-15 and SBA-16 materials on toluene oxidation. Microporous Mesoporous Mater 2013;177:97–104. https://doi.org/10.1016/j.micromeso.2013.04.024.
[32] Monte M, Gamarra D, López Cámara A, Rasmussen SB, Gyorffy N, Schay Z, et al. Preferential oxidation of CO in excess H_2 over CuO/CeO_2 catalysts: performance as a function of the copper coverage and exposed face present in the CeO_2 support. Catal Today 2014;229:104–13. https://doi.org/10.1016/j.cattod.2013.10.078.
[33] Gómez LE, Miró EE, Boix AV. Spectroscopic characterization of Mn-Co-Ce mixed oxides, active catalysts for COPROX reaction. Int J Hydrogen Energy 2013;38:5645–54. https://doi.org/10.1016/j.ijhydene.2013.03.004.
[34] Gaudin P, Fioux P, Dorge S, Nouali H, Vierling M, Fiani E, et al. Formation and role of Cu^+ species on highly dispersed CuO/SBA-15 mesoporous materials for SO_x removal: an XPS study. Fuel Process Technol 2016;153:129–36. https://doi.org/10.1016/j.fuproc.2016.07.015.
[35] Gamarra D, Munuera G, Hungría AB, Fernández-García M, Conesa JC, Midgley PA, et al. Structure-activity relationship in nanostructured copper-ceria-based preferential CO oxidation catalysts. J Phys Chem C 2007;111:11026–38. https://doi.org/10.1021/jp072243k.
[36] Mariño F, Descorme C, Duprez D. Supported base metal catalysts for the preferential oxidation of carbon monoxide in the presence of excess hydrogen (PROX). Appl Catal B Environ 2005;58:175–83. https://doi.org/10.1016/j.apcatb.2004.12.008.
[37] Di Benedetto A, Landi G, Lisi L, Russo G. Role of CO_2 on CO preferential oxidation over CuO/CeO_2 catalyst. Appl Catal B Environ 2013;142–143:169–77. https://doi.org/10.1016/j.apcatb.2013.05.001.
[38] Gu C, Lu S, Miao J, Liu Y, Wang Y. Meso-macroporous monolithic $CuO\text{-}CeO_2/\gamma/\alpha\text{-}Al_2O_3$ catalysts for CO preferential oxidation in hydrogen-rich gas: effect of loading methods. Renew Energy 2010;35:6113–22. https://doi.org/10.1016/j.ijhydene.2010.03.105.